Modeling integrated quantum frequency processors towards robust quantum networks

Benjamin E. Nussbaum[a], Andrew J. Pizzimenti[b], Navin B. Lingaraju[c], Hsuan-Hao Lu[d], and Joseph M. Lukens[d,e]

[a]Illinois Quantum Information Science & Technology Center (IQUIST), Department of Physics, University of Illinois Urbana–Champaign, Urbana, IL, USA
[b]James C. Wyant College of Optical Sciences, University of Arizona, Tucson, AZ, USA
[c]SRI International, Arlington, VA, USA
[d]Quantum Information Science Section, Oak Ridge National Laboratory, Oak Ridge, TN, USA
[e]Research Technology Office, Arizona State University, Tempe, AZ, USA

ABSTRACT

Frequency-encoded quantum information offers intriguing opportunities for quantum communications networks, with the quantum frequency processor (QFP) paradigm promising scalable construction of quantum gates. Yet all experimental demonstrations to date have relied on discrete fiber-optic components that occupy significant physical space and impart appreciable loss. We introduce a model for designing QFPs comprising microring resonator-based pulse shapers and integrated phase modulators. We estimate the performance of frequency-bin Hadamard gates, finding high fidelity values sustained for relatively wide-bandwidth frequency bins. Our simple model and can be extended to other material platforms, providing a design tool for future frequency processors in integrated photonics.

Keywords: Quantum computing, quantum networks, silicon photonics, optical pulse shaping, photonic integrated circuits, optical resonators, phase modulation

1. INTRODUCTION

Frequency encoding is emerging as a promising paradigm for photonic quantum information, for which the quantum frequency processor (QFP) has been introduced and analytically shown capable of scalable universal quantum gates.[1] The QFP's potential has been demonstrated in several fiber-optic experiments on fundamental quantum gates,[2–4] Bell-state measurements,[5] and classical communications and networking.[6,7] All QFP experiments so far have relied on concatenations of alternating commercial Fourier-transform pulse shapers and electro-optic phase modulators (EOMs) that have facilitated excellent agreement with theory. Yet the use of discrete components has proven limiting in several significant ways, including spectral resolution, insertion loss, and device footprint (~ 1 m^2). Photonic integrated circuits (PICs) offer the potential to surpass these limitations, but PIC models that incorporate the nuances of integrated microring resonator (MRR) pulse shapers on QFP gate performance have not been developed. Here we summarize recent work formulating and analyzing a complete model for PIC-based QFPs.[8] Accounting for the impact of MRRs on crosstalk and dispersion, our model connects geometric and material properties to quantum gate performance. Focusing on the frequency-bin Hadamard gate realized in silicon as a paradigmatic example, we show that peak gate fidelity values $\mathcal{F} > 1 - 10^{-7}$ are attainable, with reasonable performance for inputs whose spectral bins fill up to $\sim 10\%$ of each MRR line.

Our approach can be adapted to any material platform and provides an important foundation for the design of frequency-processing PICs that exceed the performance of their discrete counterparts—a promising outlook for the scalable growth of robust quantum networks using inexpensive, compact, and high-performance QFPs.

Corresponding authors:
B.E.N.: bn9@illinois.edu
J.M.L.: joseph.lukens@asu.edu

2. INTEGRATED QFP MODEL

Consider a collection of frequency modes centered at equispaced bins $\omega_n \triangleq \omega_0 + n\Delta\omega$ ($n \in \mathbb{Z}$), each described by a continuum of annihilation operators $\hat{a}_n(\Omega) \triangleq \hat{a}(\omega_n + \Omega)$ with $\Omega \in \left(-\frac{\Delta\omega}{2}, \frac{\Delta\omega}{2}\right)$. In contrast to most previous QFP work,[1] we explicitly include dependence on the frequency offset Ω, which will prove to be important when considering finite linewidth effects below. The QFP operates on these modes with an alternating series of EOMs and line-by-line pulse shapers. The EOMs are modeled as time-domain phase shifters that map input operators $\hat{a}_n$ to outputs $\hat{b}_m$ according to

$$\hat{b}_m(\Omega) = \sum_{n=-\infty}^{\infty} c_{m-n}\hat{a}_n(\Omega) \tag{1}$$

where $c_n = \frac{1}{T}\int_0^T \mathrm{d}t\, e^{i\varphi(t)}e^{in\Delta\omega t}$ and the phase function $\varphi(t)$ is periodic at the inverse mode spacing $T = \frac{2\pi}{\Delta\omega}$. A line-by-line pulse shaper performs the transformation $\hat{b}_n(\Omega) = e^{i\phi_n}\hat{a}_n(\Omega)$.

As long as Eq. (1) holds for each EOM, only frequencies with the same offset Ω will interfere, so that the QFP can be modeled as performing a continuum of simultaneous transformations described by matrices $V(\Omega)$ such that the final output is

$$\hat{b}_m(\Omega) = \sum_{n=-\infty}^{\infty} V_{mn}(\Omega)\hat{a}_n(\Omega) \tag{2}$$

for each offset comb defined by frequencies $\omega_n + \Omega$ ($n \in \mathbb{Z}$). Defining the $d \times d$ matrix W as the submatrix of V in the logical space of interest,[1] we can then compute the fidelity

$$\mathcal{F}_W(\Omega) = \frac{\left|\mathrm{Tr}\left[W^\dagger(\Omega)U\right]\right|^2}{d^2\mathcal{P}_W(\Omega)} \tag{3}$$

and success probability

$$\mathcal{P}_W(\Omega) = \frac{\mathrm{Tr}\left[W^\dagger(\Omega)W(\Omega)\right]}{\mathrm{Tr}\,U^\dagger U} \tag{4}$$

with respect to a targeted frequency-bin unitary U.[1,9] The explicit Ω-dependence accounts for the impact of nonuniform pulse shaper filters and is valuable when assessing integrated QFP designs.

Figure 1(a) shows the general construction of an integrated pulse shaper, where an array of MRRs isolate a pre-defined vector of M linearly spaced frequency modes centered at $\omega_m = \omega_0 + m\Delta\omega$ ($m \in \{0, 1, \ldots, M-1\}$).[10,11] The pulse shaper then applies an arbitrary phase shift φ_m to each filtered mode m. The full frequency response for an MRR-based pulse shaper can be written as

$$H(\omega) \triangleq \frac{E_{\mathrm{drop}}(\omega)}{E_{\mathrm{in}}(\omega)} = \sum_{p=0}^{M-1}\left(D_p^2(\omega)e^{i\phi_p}\prod_{\substack{q=0 \\ q\neq p}}^{M-1} T_q(\omega)\right), \tag{5}$$

where $T_p(\omega)$ $[D_p(\omega)]$ corresponds to the through-port [drop-port] field response of a single MRR tuned to frequency ω_p.[12] The discrete sum contrasts with the convolution expression for a conventional diffractive pulse shaper,[13] and the consequences for QFP gate design form the primary focus of the current analysis.
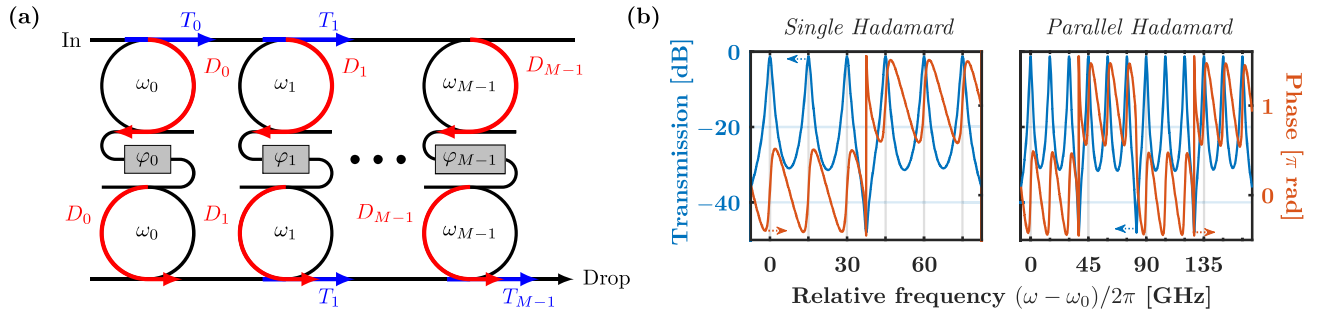

Figure 1. (a) MRR-based pulse shaper design. (b) Transmission and phase for a pulse shaper configured for use as a single (left) or parallel (right) Hadamard gate with $\frac{\Delta\omega}{2\pi} = 15$ GHz.
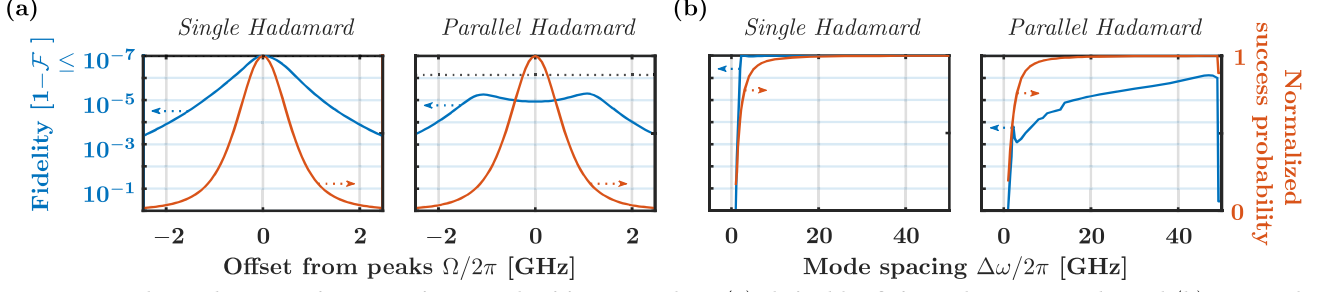
Figure 2. Hadamard gate performance for a comb of frequency bins (a) shifted by Ω from the MRR peaks and (b) centered at the transmission peaks ($\Omega = 0$) but with variable mode spacing $\Delta\omega$.

3. HADAMARD GATE PERFORMANCE

We focus on the frequency-bin Hadamard,[2, 14, 15] specifically the three-element QFP solution[16] which specifies a sinewave modulation on both EOMs (modulation index of 0.8283 rad) and a π stairstep phase shift between the logical zero and one modes on the pulse shaper. Previously, we found[2] that similar parallel Hadamard solutions incur no observable crosstalk as long as each gate is assigned six unique frequency bins: two for the logical qubit, plus two on either side as vacuum ancillas. Accordingly, we allocate $M = 6$ ($M = 12$) channels for a single (parallel) Hadamard operation in the simulations below.

Assuming operation in silicon at 300 K, a 480 nm × 220 nm waveguide cross-section, 0.5 dB cm^{-1} attenuation, and transverse-electric (TE) polarization, we design ring radii $r \approx 20$ μm and take symmetric coupling constants of 0.01 (in power) for each MRR; $\frac{\omega_0}{2\pi} = 193$ THz and $\frac{\Delta\omega}{2\pi} = 15$ GHz define the nominal frequency mode space ω_m used by the pulse shaper. As shown in Fig. 1(b), the pulse shaper response varies strongly both within and across the 15 GHz-wide bins, which emphasizes the need to define fidelity $\mathcal{F}_W(\Omega)$ and success probability $\mathcal{P}_W(\Omega)$ with respect to the ideal unitary as a function of frequency offset Ω from the peak, i.e., separately for each family of comb lines defined as $\tilde{\omega}_m = \omega_m + \Omega$. Intuitively, this definition recognizes that frequency bins experience different global operations depending on their spectral position relative to the MRR peaks. Consequently, after incorporating the mixing operations from two bookend EOMs—assumed ideal for this study (linear with negligible voltage-dependent loss)—we find the offset-dependent $\mathcal{F}_W(\Omega)$ and $\mathcal{P}_W(\Omega)$ in Fig. 2(a). Note that the latter is normalized to a peak of 0.73, due to a combination of MRR insertion loss and scattering into adjacent frequency modes. The fidelity remains above 0.9998 in both scenarios, even at a $|\Omega| = 2$ GHz; the success probability is halved with $|\Omega| = 0.6$ GHz.

In Fig. 2(b) we repeat the previous analyses for a fixed offset $\Omega = 0$ but variable $\Delta\omega$. Apart from a sharp drop for the parallel case at $\frac{\Delta\omega}{2\pi} \approx 49$ GHz, which can be attributed to crosstalk from overlapping resonances one free spectral range away,[8] both $\mathcal{F}_W$ and $\mathcal{P}_W$ generally decrease with smaller $\Delta\omega$. Significantly, $\mathcal{F}_W > 0.999$ and $\mathcal{P}_W > 0.50$ down to spacings as small as 1.85 GHz, well below the ~18 GHz practical minimum observed so far for table-top QFPs.[2] And with high-order MRR filters, even sub-GHz separations appear feasible with current technology.[8] Such integrated QFPs can also facilitate high-dimensional frequency mixers[17] furnishing new opportunities in quantum communications and networking based on frequency-bin qudits.

4. BROADBAND PERFORMANCE

The effects of frequency offset on fidelity and success probability are evident in Fig. 2. However, this frequency-offset analysis alone is not sufficient to fully predict the performance of the QFP for arbitrary, pulsed inputs which have some finite spectral extent. For broadband inputs, residual phase shifts that vary with offset will affect the overall spectro-temporal shape of the output, and must be accounted for. For example, while the spectral phases applied by the pulse shapers in Fig. 1(b) appear roughly constant at any *given* offset Ω, they vary strongly *between* offsets; therefore it is critical to quantify what impact this filtering may have on the shape of finite-linewidth inputs.

For simulation purposes, we select tunable-bandwidth inputs that satisfy the Nyquist criterion,[18–20] specifically perfect sinc pulses of the form $s(t) = \frac{T_s}{\pi t} \sin \frac{\pi t}{T_s}$, corresponding to an ideal rectangular spectrum $S(\omega)$ tunable

in width by varying the symbol frequency $\frac{1}{T_s}$:

$$S(\omega) = \begin{cases} \sqrt{\frac{T_s}{2\pi}} & |\omega| < \frac{\pi}{T_s} \\ 0 & |\omega| > \frac{\pi}{T_s} \end{cases}, \tag{6}$$

normalized such that $\int d\omega\, |S(\omega)|^2 = 1$. Although highly idealized, selection of this spectral shape is particularly convenient for bandwidth analyses, allowing us to probe the frequency response of the device under test while minimizing the potential for artifacts from features in the probe signal like spectral tails. Figure 3(a) depicts an example of the frequency comb formed by defining rectangular frequency bins according to Eq. (6). Considering computational modes (ω_2, ω_3) for the $M = 6$ Hadamard gate, we can encode a generic input qubit $|\psi\rangle = c_0 |0\rangle + c_1 |1\rangle$ as a single-photon wavepacket with complex spectrum $x(\omega) = c_0 S(\omega - \omega_2) + c_1 S(\omega - \omega_3)$.

The equations used to calculate the fidelity and success probability in the previous sections assume that the shape of the input modes is unchanged by the operation. The output wavepacket would be $g(\omega) = \tilde{c}_0 S(\omega - \omega_2) + \tilde{c}_1 S(\omega - \omega_3)$, where the new coefficients are as determined by the Hadamard gate: $[\tilde{c}_0\, \tilde{c}_1]^T = U_H [c_0\, c_1]^T$. This assumption does not hold for the broadband input model, as only a portion of the signal is located at each channel peak [cf. Fig. 3(a)]. The mode shapes $S(\omega)$ are themselves modulated by the QFP, and therefore in this section we define fidelity and success probability for the actual output wavepacket $y(\omega)$ as

$$\mathcal{F}_y = \frac{\left| \int d\omega\, g^*(\omega) y(\omega) \right|^2}{\int d\omega\, |g(\omega)|^2 \int d\omega\, |y(\omega)|^2} \tag{7}$$

and

$$\mathcal{P}_y = \frac{\int d\omega\, |y(\omega)|^2}{\int d\omega\, |g(\omega)|^2}, \tag{8}$$

where $g(\omega)$ and $y(\omega)$ are the outputs of a finite-bandwidth input that has undergone an ideal U_H and actual W transformation, respectively.

In Fig. 3(b) are the Hadamard gate $\mathcal{F}_y$ and $\mathcal{P}_y$ results for the input state $|+\rangle = \frac{1}{\sqrt{2}}(|0\rangle + |1\rangle)$, with full bandwidths ranging from 0–2 GHz, for a bin spacing $\frac{\Delta\omega}{2\pi} = 15$ GHz. Whereas the fidelity values in Fig. 2(a) remain above 0.999 over the entire peak, Fig. 3(b) shows that an input less than $\sim$60 MHz wide is required to retain the same fidelity in the pulsed case. Nonetheless, $\mathcal{F}_y > 0.99$ holds up to an input bandwidth $\sim$10% of the total MRR linewidth, an appreciable fraction for which high fidelity values should be possible experimentally.
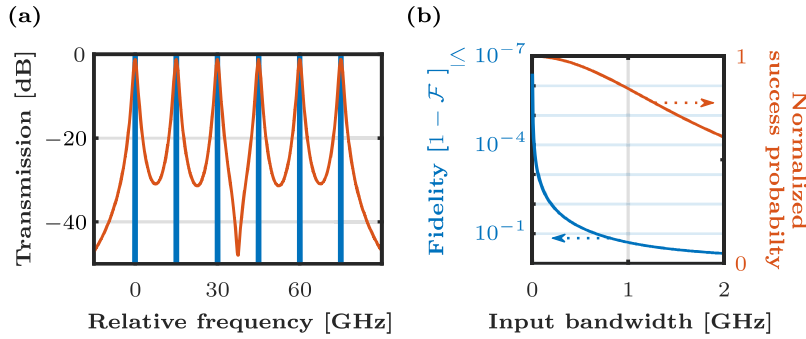

Figure 3. (a) Example Nyquist input spectrum compared to typical pulse shaper filter. The rectangular input modes are 0.97 GHz wide, equal to half the FWHM bandwidth of each pulse shaper channel. (b) Fidelity $\mathcal{F}_y$ and success probability $\mathcal{P}_y$ vs. input bandwidth for input $|+\rangle$ into a QFP Hadamard gate.

ACKNOWLEDGMENTS

REFERENCES

[1] Lukens, J. M. and Lougovski, P., "Frequency-encoded photonic qubits for scalable quantum information processing," *Optica* **4**, 8–16 (2017).

[2] Lu, H.-H., Lukens, J. M., Peters, N. A., Odele, O. D., Leaird, D. E., Weiner, A. M., and Lougovski, P., "Electro-optic frequency beam splitters and tritters for high-fidelity photonic quantum information processing," *Phys. Rev. Lett.* **120**, 030502 (2018).

[3] Lu, H.-H., Lukens, J. M., Williams, B. P., Imany, P., Peters, N. A., Weiner, A. M., and Lougovski, P., "A controlled-NOT gate for frequency-bin qubits," *npj Quantum Inf.* **5**, 24 (2019).

[4] Lu, H.-H., Simmerman, E. M., Lougovski, P., Weiner, A. M., and Lukens, J. M., "Fully arbitrary control of frequency-bin qubits," *Phys. Rev. Lett.* **125**, 120503 (2020).

[5] Lingaraju, N. B., Lu, H.-H., Leaird, D. E., Estrella, S., Lukens, J. M., and Weiner, A. M., "Bell state analyzer for spectrally distinct photons," *Optica* **9**, 280–283 (2022).

[6] Lukens, J. M., Lu, H.-H., Qi, B., Lougovski, P., Weiner, A. M., and Williams, B. P., "All-optical frequency processor for networking applications," *J. Light. Technol.* **38**, 1678–1687 (2020).

[7] Lu, H.-H., Qi, B., Williams, B. P., Lougovski, P., Weiner, A. M., and Lukens, J. M., "Agile frequency transformations for dense wavelength-multiplexed communications," *Opt. Express* **28**, 20379–20390 (2020).

[8] Nussbaum, B. E., Pizzimenti, A. J., Lingaraju, N. B., Lu, H.-H., and Lukens, J. M., "Design methodologies for integrated quantum frequency processors," *J. Light. Technol.* **40**, 7648–7657 (2022).

[9] Uskov, D. B., Kaplan, L., Smith, A. M., Huver, S. D., and Dowling, J. P., "Maximal success probabilities of linear-optical quantum gates," *Phys. Rev. A* **79**, 042326 (2009).

[10] Agarwal, A., Toliver, P., Menendez, R., Etemad, S., Jackel, J., Young, J., Banwell, T., Little, B. E., Chu, S. T., Wei Chen, Wenlu Chen, Hryniewicz, J., Johnson, F., Gill, D., King, O., Davidson, R., Donovan, K., and Delfyett, P. J., "Fully programmable ring-resonator-based integrated photonic circuit for phase coherent applications," *J. Light. Technol.* **24**, 77–87 (2006).

[11] Wang, J., Shen, H., Fan, L., Wu, R., Niu, B., Varghese, L. T., Xuan, Y., Leaird, D. E., Wang, X., Gan, F., Weiner, A. M., and Qi, M., "Reconfigurable radio-frequency arbitrary waveforms synthesized in a silicon photonic chip," *Nat. Commun.* **6**, 5957 (2015).

[12] Chrostowski, L. and Hochberg, M., [*Silicon Photonics Design: From Devices to Systems*], Cambridge University Press (2015).

[13] Weiner, A. M., [*Ultrafast Optics*], Wiley (2009).

[14] Kobayashi, T., Ikuta, R., Yasui, S., Miki, S., Yamashita, T., Terai, H., Yamamoto, T., Koashi, M., and Imoto, N., "Frequency-domain Hong–Ou–Mandel interference," *Nat. Photon.* **10**, 441–444 (2016).

[15] Clemmen, S., Farsi, A., Ramelow, S., and Gaeta, A. L., "Ramsey interference with single photons," *Phys. Rev. Lett.* **117**, 223601 (2016).

[16] Lu, H.-H., Klco, N., Lukens, J. M., Morris, T. D., Bansal, A., Ekström, A., Hagen, G., Papenbrock, T., Weiner, A. M., Savage, M. J., et al., "Simulations of subatomic many-body physics on a quantum frequency processor," *Phys. Rev. A* **100**, 012320 (2019).

[17] Lu, H.-H., Lingaraju, N. B., Leaird, D. E., Weiner, A. M., and Lukens, J. M., "High-dimensional discrete Fourier transform gates with a quantum frequency processor," *Opt. Express* **30**, 10126–10134 (2022).

[18] Nakazawa, M., Hirooka, T., Ruan, P., and Guan, P., "Ultrahigh-speed 'orthogonal' TDM transmission with an optical Nyquist pulse train," *Opt. Express* **20**, 1129–1140 (2012).

[19] Soto, M. A., Alem, M., Shoaie, M. A., Vedadi, A., Brès, C.-S., Thévenaz, L., and Schneider, T., "Optical sinc-shaped Nyquist pulses of exceptional quality," *Nat. Commun.* **4**, 2898 (2013).

[20] Leuthold, J. and Brès, C.-S., "All-optical pulse shaping for highest spectral efficiency," in [*All-Optical Signal Processing*], 217–260, Springer (2015).